





Conversion of a basis-dependent superposition of orbital-angular-momentum states using a q plate

Sarvesh Bansal ^{*}, Sushanta Kumar Pal , and P. Senthilkumaran 

Department of Physics, Indian Institute of Technology Delhi, Hauz Khas, New Delhi 110016, India

 (Received 26 February 2021; revised 28 June 2021; accepted 12 July 2021; published 3 September 2021)

Stokes parameters play a vital role in the study of photons, electrons, and other elementary particles. Superposition of phase singularities in an orthogonal polarization basis leads to the creation of Stokes singularities. It has been established that these phase singularities carry orbital angular momentum of light and hence the study of Stokes singularities is significant. The superposition of orbital-angular-momentum states, depending on the chosen basis, leads to the formation of different types of Stokes singularities such as polarization singularities and Poincaré singularities. These are subsets of Stokes singularities. There is a plethora of applications that has emerged in recent years for both phase and polarization singularities. Spin to orbital-angular-momentum conversion is possible by the use of a q plate. In fact, a q plate can convert a scalar beam into a phase or polarization vortex and a polarization singularity into another polarization singularity. But the process of the inter- or intraconversion of Stokes vortices has not been reported so far. This article discusses this aspect and the invariance of various topological parameters that occur in this process.

DOI: [10.1103/PhysRevA.104.033503](https://doi.org/10.1103/PhysRevA.104.033503)

I. INTRODUCTION

Photons possess integral spin and they carry spin angular momentum of $\pm\hbar$ per photon. In addition to spin angular momentum (SAM), photons can possess orbital angular momentum [1,2]. In light fields, spin angular momentum (SAM) is attributed to the polarization of light and orbital angular momentum (OAM) is attributed to the helical phase structure of the scalar vortices, also called phase singularities. Superposition of such scalar vortex beams, each in different polarization state results in the formation of Stokes singularities. In beams containing Stokes singularities, the polarization distribution is inhomogeneous but structured, and since they are vortex superpositions the study of OAM in such beams is important. Also, there are many ways orthogonal polarization states can be chosen and superpositions can be realized. If the chosen basis states are right and left circularly polarized states, the superposition results in polarization singularities also called spin-orbit beams. However, a more general formalism is that of Stokes singularities that are the superposition of orthogonal polarization and orbital-angular-momentum states. Therefore, Stokes singularities form a universal set in which polarization, Poincaré, and phase singularities are subsets. Topological invariances such as charge conservation in scalar vortices and index conservation in polarization singularities have been reported in the literature. Sign rules are stated for both scalar and polarization singularities [3]. In this article, while presenting inter- and intraconversion of Stokes singularities, conservation of Stokes index, angular momentum, and sign rules are dealt. The subject is developed by providing the required background in this section.

A. Stokes parameters and Stokes fields

The state of polarization (SOP) of an optical beam can be represented in terms of four measurable quantities, known as Stokes parameters [4]:

$$\begin{aligned} S_0 &= I_x + I_y, \\ S_1 &= I_x - I_y, \\ S_2 &= I_D - I_A, \\ S_3 &= I_R - I_L, \end{aligned} \quad (1)$$

where I_x , I_y , I_D , I_A , I_R , and I_L are the component intensities in x , y , diagonal, antidiagonal, right circular, and left circular states, respectively. The Stokes parameters play a vital role in the study of photons, electrons, and other elementary particles. Stokes parameters can also be expressed in terms of Pauli's spin matrices [5] as

$$\begin{aligned} S_0 &= [a_x^* \quad a_y^*] I \begin{bmatrix} a_x \\ a_y \end{bmatrix} = a_x a_x^* + a_y a_y^*, \\ S_1 &= [a_x^* \quad a_y^*] \sigma_z \begin{bmatrix} a_x \\ a_y \end{bmatrix} = a_x a_x^* - a_y a_y^*, \\ S_2 &= [a_x^* \quad a_y^*] \sigma_x \begin{bmatrix} a_x \\ a_y \end{bmatrix} = a_x a_y^* + a_y a_x^*, \\ S_3 &= [a_x^* \quad a_y^*] \sigma_y \begin{bmatrix} a_x \\ a_y \end{bmatrix} = i(a_x a_y^* - a_y a_x^*), \end{aligned} \quad (2)$$

where a_x and a_y are transverse field components. Both a_x and a_y are complex quantities. I is a 2×2 identity matrix and σ_x , σ_y , and σ_z are 2×2 Pauli spin matrices. We can see that, for a given SOP, under three commonly employed orthogonal decompositions, the component intensity differences

^{*}bansalsarvesh.s@gmail.com

constitute the Stokes parameters. To include the component field phase differences, the Stokes field formalism can be employed, which is explained below.

Using any two Stokes parameters out of S_1 , S_2 , and S_3 , mathematical fields called Stokes fields can be constructed [3,6] and they are given as

$$S_{\alpha\beta} = S_\alpha + iS_\beta, \quad (3)$$

where $\alpha, \beta = 1, 2, 3$ and $\alpha \neq \beta$. The phase distribution of Stokes field $S_{\alpha\beta}$ can be expressed as

$$\phi_{\alpha\beta} = \arctan(S_\beta/S_\alpha). \quad (4)$$

For homogeneously polarized fields, $S_{\alpha\beta}$ is a phasor, whereas for the inhomogeneously polarized field this represents Stokes field. The mathematically constructed S_{12} Stokes field is made up of intensity measurements in linear states, namely I_x , I_y , I_D , and I_A , but surprisingly S_{12} Stokes field provides the information about the phase difference between circular basis states. Likewise, Stokes fields S_{23} and S_{31} also can be shown to provide the phase difference between corresponding orthogonal basis states [7]:

$$\begin{aligned} \arg(S_1 + iS_2) &= \phi_{12} = \phi_L - \phi_R, \\ \arg(S_2 + iS_3) &= \phi_{23} = \phi_y - \phi_x, \\ \arg(S_3 + iS_1) &= \phi_{31} = \phi_A - \phi_D. \end{aligned} \quad (5)$$

Stokes phase can be controlled by changing the birefringence (either circular or linear) of the medium through which the optical fields propagate. Both the Stokes parameters and Stokes fields appear in coherency matrix C as diagonal and off-diagonal elements, respectively,

$$C_{xy} = \begin{bmatrix} S_0 + S_1 & S_{23}^* \\ S_{23} & S_0 - S_1 \end{bmatrix}. \quad (6)$$

The other Stokes parameters and fields also appear in the coherency matrix, expressed under different bases. For diagonal (DA) and circular bases (LR) the coherency matrices are given by

$$\begin{aligned} C_{DA} &= \begin{bmatrix} S_0 + S_2 & iS_{31}^* \\ iS_{31} & S_0 - S_2 \end{bmatrix}, \\ C_{LR} &= \begin{bmatrix} S_0 + S_3 & S_{12}^* \\ S_{12} & S_0 - S_3 \end{bmatrix}. \end{aligned} \quad (7)$$

The Stokes parameters and Stokes fields define the elements of the coherency matrix [8,9], which also corresponds to the quantum-mechanical density matrix for an ensemble of photons. Density matrices are useful to represent mixed states, which offer less than maximum information, normally offered by pure states. Classical concepts such as Stokes parameters and Poincaré sphere can also be applied to the quantum world, but due to the fluctuations in the number of photons the Poincaré sphere is transformed into Poincaré space, which is a set of concentric nested spheres. Also, the fluctuations lead to the description of higher-order moments of the Stokes parameters, which is absent in the classical picture [10]. Nevertheless, Stokes parameters can be immediately translated into the quantum realm [11–13], using noncommuting Stokes operators. Also, while going from pure state to mixed

states, density matrix (coherency matrix) formalism is useful. Concepts of density or coherency matrix are mentioned here to bring out the importance of Stokes fields and the Stokes formalism and we follow a classical approach and stick to pure states here in this paper. In a pure state, the diagonal and the off-diagonal elements of the density matrix can be interpreted as providing intensity and phase information, respectively. This relative phase has been referred to as Stokes phase in literature [5,7,11,14–18]. For inhomogeneously polarized light beams, the Stokes phase is a distribution. The singularities present in Stokes phase distribution are called Stokes singularities or Stokes vortices.

B. Singularities: Phase and Stokes singularities

Singularities: Singularity refers to situations where a parameter defining a physical entity blows up or becomes indeterminate. Point singularities are ubiquitous and have their signatures in various physical phenomena around us [17,18]. It is also associated with circular motion about the singular point (vortex core) in a two-dimensional field [19]. In three dimension vortex core draws a curve forming a tube, like in tornadoes. In this subsection the singularities in complex fields, phase distributions, and polarization distributions are introduced. In a two-dimensional complex plane, according to the Cauchy integral theorem, a singularity is defined by the contour integral $\oint f(z)dz = 2\pi iR$, being nonzero, where R is a residue. The complex field does not satisfy Cauchy-Riemann conditions, indicating that the field is not analytic and line integrals between any two points have path dependence. The phase singularities are basically the singularities that appear in the phase distribution of a complex field. This means that $\oint \nabla\phi \cdot dl = 2\pi m$, where m is called the winding number or topological charge of the phase singularity. For example, among the two complex functions $f_1(z) = x + iy = r \exp(i\phi)$ and $f_2(z) = x - iy = r \exp(-i\phi)$, function f_1 is analytic, whereas f_2 has a singularity at the origin. But both the functions have a singularity in their phase distribution as $\oint \nabla\phi \cdot dl = 2\pi m$. For the function f_1 the topological charge m is $+1$, whereas for f_2 it is -1 . Similarly, polarization singularities are the locations at which the polarization azimuth $\gamma = 0.5 \arctan(S_2/S_1)$ is undefined and the line integral $\oint \nabla\gamma \cdot dl \neq 0$. The polarization singularity indices are defined later in the introduction. Note that, in these three cases, the line integral is on complex function $f(z)$, phase gradient $\nabla\phi$, and azimuth gradient $\nabla\gamma$, respectively. In fluids, it is the velocity vector field where circulations are present if there are vortices (singularities) [20]. Like the velocity field, in a phase singularity the phase gradient field and in a polarization singularity the azimuth gradient field are solenoidal. Hence in a singularity the parameter under consideration is undefined at the singular point and, in its neighbourhood, the gradient is circulating.

OAM and phase singularities: The energy flow in optical fields can be studied in terms of Poynting vector \vec{S} (energy flux density also called current density j) defined by

$$\vec{S} = \frac{1}{\mu_0} \vec{E} \times \vec{B}, \quad (8)$$

where \vec{E} and \vec{B} are electric and magnetic fields of electromagnetic wave and μ_0 is the permeability of free space. The continuity equation for the flow of energy is given by $\partial\mathcal{E}/\partial t = -\nabla \cdot \vec{S}$, where \mathcal{E} is the energy density [21]. This flow can also be expressed in terms of phase gradients [22] as phase gradient vector gives the propagation vector. Considering a complex scalar optical field $\psi = r \exp(i\phi) = \zeta + i\xi$, the optical current \vec{j} is given by

$$\vec{j} = I\nabla\phi, \quad (9)$$

where $I = \psi\psi^*$ is the intensity and ψ^* is the conjugate of ψ . The real and imaginary part of the complex field is given by ζ and ξ , respectively. The phase of the field can be written as $\phi = \text{Im}[\log\psi]$. Using this in Eq. (9), the optical current can be given by

$$\vec{j} = \text{Im}[\psi^*\nabla\psi] = \frac{i}{2}(\psi^*\nabla\psi - \psi\nabla\psi^*) = \zeta\nabla\xi - \xi\nabla\zeta. \quad (10)$$

For a plane wave in free space, the optical current is in the direction of propagation. But for an optical field consisting of a phase singularity, the transverse component of the phase gradient is circulating and, together with the longitudinal component, the flow is helical, winding, and advancing along the vortex core [23–25]. This circulation is responsible for the OAM in light beams. In singular optics, it is now well established that phase singular beams carry OAM [1]. The OAM in light beams can also be understood by looking at the analogy between the paraxial wave equation with the Schrödinger wave equation [26,27]. The operator corresponding to the z component of orbital angular momentum is $L_z = -i\hbar\frac{\partial}{\partial\phi}$ and applying this to beams having azimuthal phase dependence like $\exp(i\ell\phi)$ gives an orbital-angular-momentum component of $\ell\hbar$ to phase singular beams.

Polarization singularities: Polarization singularities are the natural extension of phase singularities, as they can be constructed by superposition of phase singularities in orthogonal polarization basis states. Depending on polarization distribution, polarization singularities are categorized into two types: (a) ellipse field (C-point) singularities and (b) vector field (V-point) singularities. For the ellipse field, azimuth pertains to the orientation of the major axis of the polarization ellipse and singularity is assigned an index $I_c = \Delta\gamma/2\pi$. For vector fields, azimuth pertains to the orientation of linear polarization, and singularity occurring in the vector field is assigned an index called the Poincaré-Hopf index and is given by $\eta = \Delta\gamma/2\pi$. Among polarization singularities C-point singularities have handedness, whereas V-point singularities do not have handedness.

OAM without vortices is also possible due to spatially varying polarization distribution [28]. By decomposing the spatially varying polarization into component distributions the presence of vortices may show up as Stokes vortices [29]. Even in scalar optics, OAM without helical wave front is shown possible by locally engineering the wave-front tilts [30–32]. In such cases, by circular harmonic decomposition [33,34] of the resultant wave front, the presence of vortices can be discerned even though the optical field does not openly reveal the presence of helical phase term [$\exp(i\ell\phi)$], which is attributed to OAM, in it.

Stokes singularities: Phase distribution of the complex Stokes fields defined by Eq. (3) can have singularities known as Stokes vortices [35]. These vortices also obey the sign rules similar to optical vortices. In the $S_{\alpha\beta}$ Stokes field, the Stokes vortex lies on the intersection of zero crossing of S_α and S_β . Stokes vortices are characterized by Stokes index given as

$$\sigma_{\alpha\beta} = \frac{\Delta\phi_{\alpha\beta}}{2\pi}, \quad (11)$$

where $\Delta\phi_{\alpha\beta}$ is accumulated Stokes phase around the Stokes vortices and can be given by

$$\Delta\phi_{\alpha\beta} = \oint \nabla\phi_{\alpha\beta} \cdot \vec{dl}. \quad (12)$$

The Stokes index $\sigma_{\alpha\beta}$ can have positive or negative integral value. The appearance of all three Stokes vortices are interlinked as they are representing the same polarization distribution. So they cannot be inconsistent with each other. If the polarization distribution undergoes a change, then all three Stokes vortices have to undergo appropriate changes. Vortices of S_{12} are referred to as polarization singularities [36,37], whereas vortices of S_{23} and S_{31} are referred to as Poincaré singularities. For polarization singularity $\sigma_{12} \neq 0$ and if $S_3 \neq 0$, then the singularity is ellipse field singularity also known as C-point singularity that can be represented by a point on a hybrid order Poincaré sphere (HyOPS). The C-point index I_c is defined as $I_c = \sigma_{12}/2$. When $\sigma_{12} \neq 0$ and $S_3 = 0$, the singularity is vector field singularity also known as V-point singularity. It is characterized by Poincaré-Hopf index η defined as $\eta = \sigma_{12}/2$. In S_{12} Stokes singularities the azimuth is not defined at the singular points. At S_{23} and S_{31} Stokes singularities, apart from satisfying the condition given by Eq. (11), the handedness is not defined at the singular points. SOP at S_{23} is either horizontal or vertical ($S_1 = \pm 1$) and SOP at S_{31} is either diagonal or antidiagonal ($S_2 = \pm 1$). Both these singularities are surrounded by polarization of varying ellipticity and azimuth. Pure vector fields with $S_3 = 0$ do not host S_{23} and S_{31} Stokes vortices and hence we restrict our study here only to S_{12} fields with no restriction on the S_3 parameter. Such beams are called Poincaré beams [38–40] and they have been studied because of their applications in various fields [41–48].

Recently, a few studies [29,40] have presented methods to generate all three Stokes vortices in the same field simultaneously. These studies show the generation of Stokes vortices using two or multiple beams interference. But so far inter- and intraconversion of Stokes vortices have not been discussed. In this article we present a method (1) for interconversion of Stokes vortices, (2) for the intraconversion among Stokes vortices, (3) to change spatial positions of Stokes vortices, and (4) to change the number of Stokes vortices embedded in the beam. Further, (5) the conservation of fundamental quantities or aspects such as Stokes index, sign rule, and angular momentum are discussed as the beam undergoes a change during the above listed conversions of Stokes vortices. The importance of a q plate which couples spin and orbital angular momentum is studied as it plays a role in interconversion between and among bright and dark Stokes vortices.

II. THEORY AND DISCUSSIONS

One of the ways of realizing all three Stokes vortices is by the superposition of beams in two orthogonal circular bases—one or both carrying orbital angular momentum and given by

$$\vec{E}(r, \theta) = Ar^{|m|}\exp(im\theta)\hat{e}_L + Br^{|n|}\exp[i(n\theta + \theta_0)]\hat{e}_R, \quad (13)$$

where \hat{e}_L and \hat{e}_R are left and right circular unit basis vectors, respectively. In Eq. (13), r is radial coordinate, θ is azimuthal angle, and θ_0 is initial phase shift given to one of the beams. m , n are the topological charges of the phase vortex beams with amplitude scaling factors A and B , respectively. The intrinsic orbital angular momentum (OAM) carried by orthogonal spin angular momentum (SAM) components are $m\hbar$ and $n\hbar$ per photon. Here, left- (right-) handed circularly polarized light carries SAM equal to $+\hbar$ ($-\hbar$) per photon. The Stokes singularity index of the singularity presented by Eq. (13) can be given as $(n - m)$. For $|m| \neq |n|$, Eq. (13) gives Poincaré beams with C points at the center of the beams. The Stokes vortex is dark if both m and n are nonzero and is bright if either m or n is zero [36,40,49]. In Poincaré beams formed in circular basis superposition, the S_{23} and S_{31} Stokes vortices lie on a closed L line around the C point as shown in Fig. 1. For each beam with specific SOP distribution, six different attributes are presented in Fig. 1. They are SOP distribution, zero contour map, intensity distribution, and three Stokes phase distributions. Figure 1(a1) depicts the polarization distribution of the incident beam carrying C point of polarization singularity index $I_c = 1/2$ at the center of the beam, which coincides with origin. Zero contours of S_1 , S_2 , and S_3 are given in Fig. 1(a2). The phase distributions of S_{12} , S_{23} , and S_{31} Stokes fields are shown in Figs. 1(a3)–1(a5), respectively. It can be seen from Fig. 1(a3) that S_{12} Stokes phase is embedded with a phase singularity of charge $+1$. Both S_{23} and S_{31} Stokes phase distributions as shown in Figs. 1(a4) and 1(a5) are embedded with two phase singularities of charge ± 1 which lie on zero contour of S_3 (L line). The (SOP) at S_{23} (S_{31}) Stokes vortices are horizontal or vertical ($+45^\circ$ or -45°) linear states that occur when the amplitudes of the two component vortex beams are the same and the phase difference between two component vortex beams are $p\pi$ for S_{23} Stokes vortices [$(p + 1/2)\pi$ for S_{31} Stokes vortices], where p is an integer. Condition on phase for these two (S_{23} and S_{31}) field vortices on the ring can be written as

$$(m - n)\theta - \theta_0 = p\pi \quad \text{or} \quad (p + 1/2)\pi, \quad (14)$$

which can be further simplified as

$$y = x \tan \left\{ \frac{p\pi + \theta_0}{m - n} \right\} \quad \text{or} \quad y = x \tan \left\{ \frac{(p + 1/2)\pi + \theta_0}{m - n} \right\}. \quad (15)$$

Likewise condition on amplitudes of orthogonal components can be written as $Ar^{|m|} = Br^{|n|}$ at these singular points. Amplitude and phase conditions can be used to find the locations of S_{23} vortices and are given as

$$\begin{aligned} x &= \left(\frac{B}{A}\right)^{(|n|-|m|)} \cos \left\{ \frac{p\pi + \theta_0}{m - n} \right\}, \\ y &= \left(\frac{B}{A}\right)^{(|n|-|m|)} \sin \left\{ \frac{p\pi + \theta_0}{m - n} \right\}. \end{aligned} \quad (16)$$

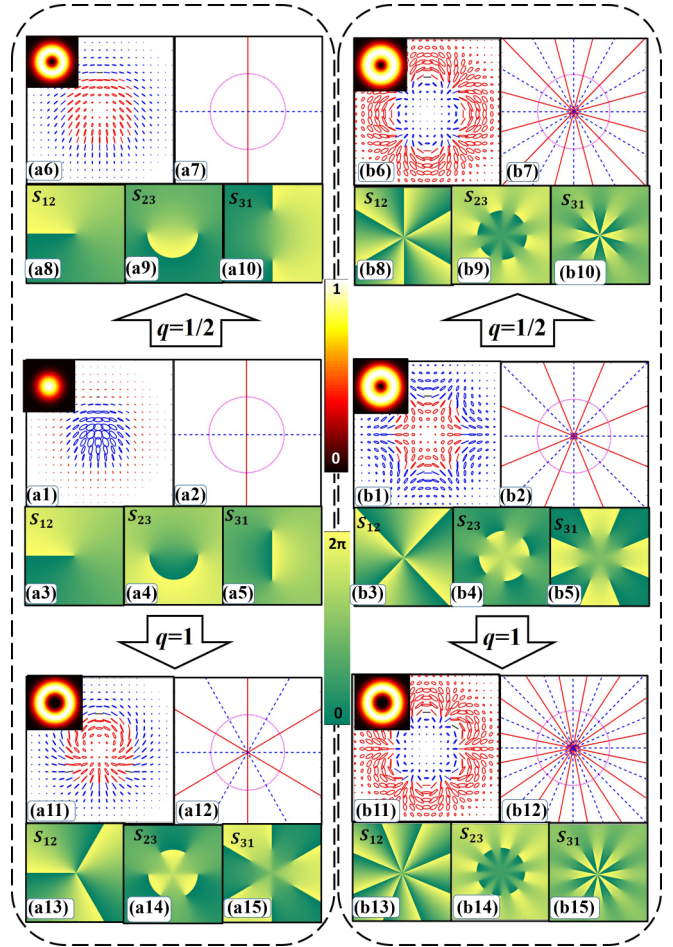


FIG. 1. Intraconversion of S_{12} Stokes vortex: for each beam in circular basis superposition, there are six different attributes, namely SOP distribution, intensity distribution, zero contour map [S_1 (red line), S_2 (blue line), and S_3 (pink line)], and three different Stokes phase distributions. The input beam is given in the middle row. When this beam is passed through a q plate with $q = 1/2$ and $q = 1$ the emerging beams are presented in the upper row and bottom row, respectively. For incident C points (a1) $m = 0$ and $n = 1$ and (b1) $m = 3$ and $n = -1$, where m and n are OAM values carried by LCP and RCP components, respectively, in the superposition. All C points are generated for $A = B$ and $\theta_0 = 0$ in Eq. (8).

Similarly, S_{31} Stokes vortices can be located at

$$\begin{aligned} x &= \left(\frac{B}{A}\right)^{(|n|-|m|)} \cos \left\{ \frac{(p + 1/2)\pi + \theta_0}{m - n} \right\}, \\ y &= \left(\frac{B}{A}\right)^{(|n|-|m|)} \sin \left\{ \frac{(p + 1/2)\pi + \theta_0}{m - n} \right\}. \end{aligned} \quad (17)$$

From Eqs. (16) and (17) it can be seen that both S_{23} and S_{31} Stokes vortices lie on a ring with radius equal to $(B/A)^{(|n|-|m|)}$ as shown by the pink line in Fig. 1(a2). If the amplitude factors A and B are equal then the ring will be always of unit radius irrespective of OAM content of the beams. We can increase or decrease the radius of the ring by changing the amplitude factors A and B . Phase shift θ_0 can be used to

rotate Stokes vortices over the ring. For S_{23} Stokes vortices the parameter p can take integer values only for $\theta = 0$ (horizontal) and $\theta = \pi$ (vertical). Therefore, the number of S_{23} Stokes vortices on the rings are $2|m - n|$ or $4|I_c|$ or $2|\sigma_{12}|$, which can be verified from Fig. 1. Similarly, for S_{31} Stokes vortices the parameter p will have integer values for $\theta = \pi/2$ and $\theta = 3\pi/2$. The number of S_{31} Stokes vortices on the ring will be $2|m - n|$ or $4|I_c|$ or $2|\sigma_{12}|$. The total number of Stokes vortices on the ring will be $8|I_c|$ or $4|\sigma_{12}|$ and the total number of Stokes vortices in the optical field will be

$$TN = 1(S_{12}) + 2|\sigma_{12}|(S_{23}) + 2|\sigma_{12}|(S_{31}). \quad (18)$$

In Fig. 1(a2) zeros of S_1 , S_2 , and S_3 are shown. The Stokes vortices of S_{23} occur at points, at which $S_2 = 0$ contour crosses $S_3 = 0$ contour. The Stokes index σ_{23} of these vortices alternates sign along the $S_2 = 0$ contour or $S_3 = 0$ contour. A similar sign rule holds good for S_{31} Stokes vortices along $S_3 = 0$ contour or $S_1 = 0$ contour. According to the sign rule, total index of Stokes vortices on the closed zero contour of S_α is zero. The index of Stokes vortex inside this closed zero contour (ring) is nonzero, which can be verified from Fig. 1(a2). There are two S_{23} Stokes vortices on $S_3 = 0$ contour (pink line) with Stokes index $\sigma_{23} = \pm 1$. So, net Stokes index is zero, in compliance with sign rule. Similarly, there are two S_{31} Stokes vortices on $S_3 = 0$ contour with alternate Stokes index sign. The net S_{31} Stokes index is zero. In this case, $\nabla\phi_{12}$ vector points along $S_3 = 0$ contour and ϕ_{12} varies between zero and $(\sigma_{12} \times 2\pi)$. In general, the Stokes phase gradient $\nabla\phi_{\beta\gamma}$ points along $S_\alpha = 0$ contour and the accumulated Stokes phase along a closed $S_\alpha = 0$ contour equals $(\sigma_{\beta\gamma} \times 2\pi)$, with the condition on indices that $\alpha \neq \beta \neq \gamma$. In the next section, the conservation of sign rule during inter- and intraconversion of Stokes vortices is discussed.

A. Intraconversion of S_{12} Stokes vortices using a q plate

A spatially varying half wave plate or a q plate is made by segments of half wave plates (HWP), with each segment having different fast axis orientation [50–53]. Also, q plates can be made by nanostructured metasurface [54] or by arranging liquid crystals [55,56] in desired formation. A q plate converts a right (left) circularly polarized plane wave to left (right) circularly vortex beam [50]. It is also used to generate cylindrical vector beams from linear polarized light [51,52]. Recent studies have also shown that a q plate acts as a coupler for beams with homogeneous as well as inhomogeneous polarization [57]. q plates are also used in combination with a spiral phase plate and spatial light modulator to generate a HyOPS beam [58–60]. The Jones matrix of a q plate can be given as

$$J = \begin{bmatrix} \cos(2q\theta + \delta) & \sin(2q\theta + \delta) \\ \sin(2q\theta + \delta) & -\cos(2q\theta + \delta) \end{bmatrix}, \quad (19)$$

where θ (varies from 0 to 2π) is the azimuthal angle with respect to some reference axis (say x axis) and δ is the orientation angle of a q plate.

When a q plate given by Eq. (19) is illuminated with a beam carrying all Stokes vortices represented by Eq. (13), then the

transmitted beam is given as

$$\begin{aligned} \vec{E}'(r, \theta) &= J \vec{E}(r, \theta) \\ &= \begin{bmatrix} \cos(2q\theta + \delta) & \sin(2q\theta + \delta) \\ \sin(2q\theta + \delta) & -\cos(2q\theta + \delta) \end{bmatrix} \vec{E}(r, \theta) \\ &= Br^{|m|} \exp\{i[(n - 2q)\theta + \theta_0 - \delta]\} \hat{e}_L \\ &\quad + Ar^{|m|} \exp\{i[(m + 2q)\theta + \delta]\} \hat{e}_R. \end{aligned} \quad (20)$$

The polarization singularity index corresponding to the transmitted beam [Eq. (20)] is $(4q + m - n)/2$, where q can be positive or negative. Negative q plates can be generated either by orienting fast axis of HWP segments in star formation or by sandwiching a positive q plate between two HWPs [61]. For $|m| \neq |n|$ Eq. (20) gives a C-point polarization singular beam. Stokes index of S_{12} Stokes field for the transmitted beam is equal to $\sigma'_{12} = (4q + m - n) = 4q - \sigma_{12}$. As aforementioned, the number of S_{23} and S_{31} Stokes vortices around the C point is twice that of the Stokes index of central singularity. The generated S_{23} or S_{31} Stokes vortices from a q plate are given by the following equation:

$$N' = 2|\sigma'_{12}| = |8q - 2\sigma_{12}|. \quad (21)$$

Hence the total number of Stokes vortices in the transmitted beam through a q plate is

$$TN' = 1(S_{12}) + |8q - 2\sigma_{12}|(S_{23}) + |8q - 2\sigma_{12}|(S_{31}). \quad (22)$$

As can be seen from Eq. (21), the number of S_{23} and S_{31} Stokes vortices in the transmitted beam depends on two factors: (a) value of Stokes index of incident beam and (b) q value of q plate. So there are two ways of changing the number of Stokes vortices: (i) by changing the q value keeping incident beam fixed and (ii) by changing the Stokes index of incident beam keeping q value fixed.

Figure 1 shows the simulation results that depict the effect of sending C-point field distributions with Stokes index $\sigma_{12} = +1$ (left column) and $\sigma_{12} = -4$ (right column) through a q plate. Two q plates with $q = 1/2$ and $q = 1$ are considered here. In this figure the input beam is shown in the middle row and two cases of outputs are shown above and below the middle row. Simulation results corresponding to an incident beam embedded with C point of $I_c = +1/2$ are given in the left column of Fig. 1. Polarization distribution, zero contour map, and Stokes phases of incident beam are given in Figs. 1(a1)–1(a5). Polarization distribution, intensity, and Stokes phases of transmitted beam through $q = 1/2$ are shown in Figs. 1(a6)–1(a10). Similarly when the incident beam is passed through a $q = 1$ plate the output is shown in Figs. 1(a11)–1(a15). The change in number of generic Stokes vortices in the ring and the change in the index of the central Stokes vortex are discussed only for the case presented in the right column for brevity (although such a discussion can be repeated for the left column). Starting from the middle row of the figure, the polarization distribution of the incident beam carrying C points at the center of the beam with polarization singularity index $I_c = -2$ is shown in Fig. 1(b1). This beam after passing through a q plate with $q = 1/2$ results in a beam whose SOP distribution is given in Fig. 1(b6). Note in this process the C-point index has changed from $I_c = -2$ to $I_c = +3$. In terms of Stokes index (σ_{12}) this change is from -4

to +6. Stokes phases embedded with singularities corresponding to the transmitted beam are given in Figs. 1(b8)–1(b10). According to Eq. (21) the number of S_{23} or S_{31} Stokes vortices generated by a q plate of q value $q = 1/2$ is equal to 12, which can be verified from Fig. 1(b9) or Fig. 1(b10). Zero contours of S_1 , S_2 , and S_3 corresponding to the transmitted beam are shown in Fig. 1(b7). From the contour lines in Fig. 1(b7) it can be seen that the S_{23} and S_{31} Stokes vortices are placed alternatively on the $S_3 = 0$ ring and the S_{12} Stokes vortex is located at the center of the beam.

We can further increase the number of Stokes vortices by changing the q value of the q plate. Simulation results for the same incident beam but a q plate with q value $q = 1$ are given in Figs. 1(b11)–1(b15). Here we discuss the case of sending the input beam with SOP given in Fig. 1(b1) through a q plate. Figure 1(b11) depicts the polarization distribution of the transmitted beam. S_{12} , S_{23} , and S_{31} Stokes phases of transmitted beam are given in Fig. 1(b13), Fig. 1(b14), and Fig. 1(b15), respectively. There are sixteen S_{23} and S_{31} Stokes vortices each, as shown in Figs. 1(b14) and 1(b15), respectively, which can be verified from Eq. (21). From Fig. 1, it is interesting to note that the S_{23} and S_{31} Stokes vortices in the transmitted beam are generated in pairs (equal number of positive and negative Stokes vortices) using a q plate. As Stokes vortices are generated in pair, total angular momentum on the Stokes ring is conserved during the intraconversion process.

B. Conversion between and among bright and dark Stokes vortices

Another objective of the article is generation of bright and dark Stokes vortices and their interconversion ($S_{12} \leftrightarrow S_{23}$ or $S_{12} \leftrightarrow S_{31}$) by using a q plate and a QWP. In Eq. (13), $m = 0$ and $n = 1$ correspond to bright C point with $I_c = 1/2$ [Fig. 1(a1)]. When this beam is passed through a q plate with $q = 1$, the transmitted beam is embedded with dark C point with $I_c = 3/2$ as shown in Fig. 1(a11). The q plate has converted a bright C point into a dark C point and, since a C point is a S_{12} Stokes vortex, this conversion is a conversion of a bright Stokes vortex into a dark Stokes vortex.

Now if the transmitted beam [say Fig. 1(a11)] is passed through a quarter wave plate (QWP), the S_{12} Stokes vortex (C point) is converted into either S_{23} or S_{31} Stokes vortex depending on the QWP orientation. But during this conversion there is a concomitant rotation in the Stokes phase distributions. The other Stokes vortices on the ring also changed to different ones. This is shown in Fig. 2. When the fast axis of the QWP is oriented at 45° , the C point at the center is converted into an S_{23} vortex and other Stokes vortices on the ring also change their types. When the QWP is oriented at 90° , the Stokes vortex at the center is of S_{31} type. One can also notice that the Stokes vortex that is present on the ring is always bright and, in the process of interconversion, the one that comes to the center changes from bright to dark. In other words, the one that goes from the center to the ring also has changed from dark to bright. It is interesting to note that, even as QWP converts the Stokes field from one to another, the total number of Stokes vortices remains constant, which means that total angular momentum remains the same during interconversion.

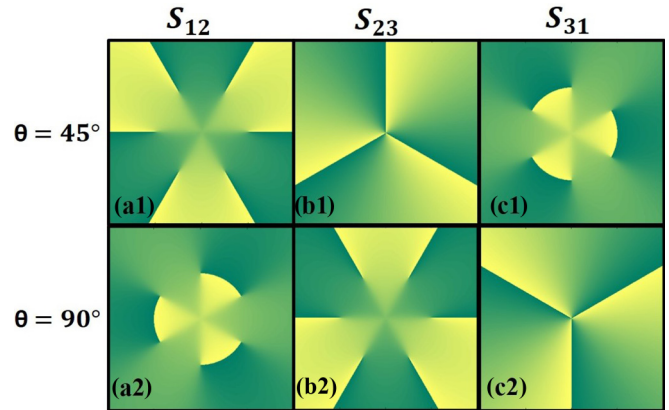


FIG. 2. Interconversion of Stokes vortices: the beam with SOP distribution given in Fig. 1(a11) is sent through a QWP oriented at angle θ . Panels (a1)–(c1) and (a2)–(c2) show the Stokes phases of S_{12} , S_{23} , and S_{31} Stokes fields of transmitted beam through QWP oriented at 45° and 90° , respectively.

C. Rotation of Stokes vortices

The fourth aim is to show the change in the spatial locations of S_{23} and S_{31} Stokes vortices on the ring. When axis of a q plate is rotated it creates an additional phase shift between two orthogonal components which in turn rotates the generated beam. Due to this Stokes vortices on the ring rotate clockwise (for clockwise rotation of a q plate) or counterclockwise (for counterclockwise rotation of a q plate). A beam with a S_{12} Stokes vortex at the center [Fig. 1(a1)] is now passed through a q plate to obtain the field depicted at Figs. 1(a13)–1(a15). When the q plate is rotated to three different angles, the changes in the Stokes phases are shown in the first, second, and third rows of Fig. 3, respectively. It can be seen that rotating a q plate by an angle of 45° can replace S_{23} and S_{31} Stokes vortices.

In general, in all the intraconversions ($S_{12} \leftrightarrow S_{12}$) or ($S_{23} \leftrightarrow S_{23}$) or ($S_{31} \leftrightarrow S_{31}$) and interconversion ($S_{12} \leftrightarrow S_{23}$ or $S_{12} \leftrightarrow S_{31}$), it can be shown that, using a q plate alone or in combination with QWP, the Stokes ring around central singularity carries an even number of Stokes vortices and the total Stokes index is zero on the ring irrespective of the type of singularity present. Note that intraconversion includes all conversions between bright and dark Stokes vortices (and among dark Stokes vortices) of the same type, where the index can be the same or raised or lowered.

III. STOKES VORTICES IN x - y AND DIAGONAL BASIS

Stokes vortices can also be generated using the superposition of two orthogonal components carrying OAM in x - y or diagonal basis. Mathematical expressions for the superposition of fields in x - y and diagonal bases for the generation of Stokes vortices are given as

$$\begin{aligned}\vec{E}_{xy}(r, \theta) &= Ar^{|u|} \exp(iu\theta) \hat{e}_x + Br^{|v|} \exp[i(v\theta + \theta_0)] \hat{e}_y, \\ \vec{E}_{DA}(r, \theta) &= Ar^{|k|} \exp(ik\theta) \hat{e}_{+45^\circ} + Br^{|l|} \exp[i(l\theta + \theta_0)] \hat{e}_{-45^\circ},\end{aligned}\quad (23)$$

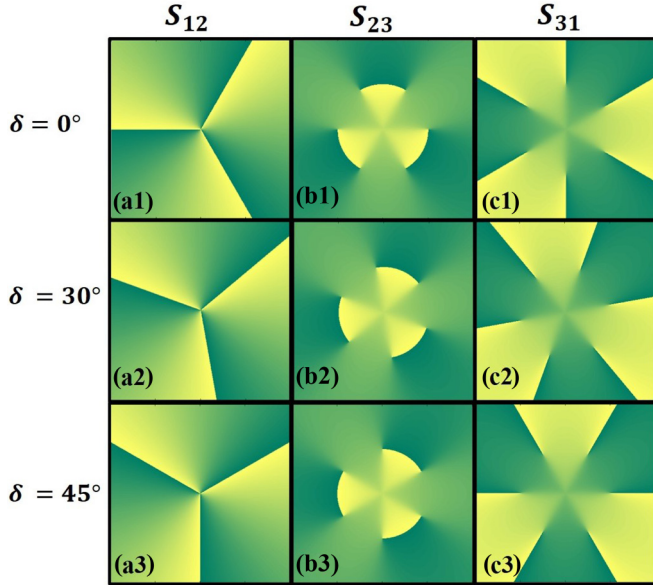


FIG. 3. Rotation of Stokes vortices: the beam with SOP distribution given in Fig. 1(a1) is sent through a rotating q plate. Panels (a1)–(c1), (a2)–(c2), and (a3)–(c3) show the Stokes phases of S_{12} , S_{23} , and S_{31} Stokes fields of the transmitted beam when the q plate is rotated by $\delta = 0^\circ$, 30° , and 45° .

where \hat{e}_x , \hat{e}_y , \hat{e}_{+45° , and \hat{e}_{-45° are the unit basis vectors along x axis, y axis, $+45^\circ$, and -45° rotated axes, respectively. u , v , k , and l are the topological charges in the respective components. Relations similar to Eq. (16) and Eq. (17) can be deduced by using Eq. (23) for these two bases. The only difference here is that S_{23} and S_{31} Stokes vortices are at the center for x - y and diagonal bases superposition, respectively, whereas other Stokes vortices will be on the ring around the central Stokes vortex like in the case of the circular basis. Simulation results for the Stokes vortices generation in the x - y basis are given in the left column of Fig. 4. Polarization distribution of the incident beam in the x - y basis is given in the middle row [Fig. 4(a1)]. S_{12} , S_{23} , and S_{31} Stokes phases for incident beams are given in Figs. 4(a3)–4(a5). It can be seen from Fig. 4(a4) that the incident beam hosts S_{23} Stokes vortex with Stokes index $\sigma_{23} = -6$ at the center. S_{12} and S_{31} Stokes phases are embedded with twelve Stokes vortices of alternate signs. Zero contours of S_1 , S_2 , and S_3 for the incident beam are given in Fig. 4(a2). From Fig. 4(a2) it can be seen that zero contour of S_1 makes the closed ring around the center singularity and S_{12} and S_{31} Stokes vortices lie alternatively on this ring. Figure 4(a6) gives the polarization distribution of the transmitted beam when the beam given in Eq. (23) is passed through the q plate of q value $q = 1/2$. S_{12} , S_{23} , and S_{31} Stokes phases for the transmitted beam are given in Figs. 4(a8)–4(a10). S_{12} , S_{23} , and S_{31} Stokes phases of transmitted beams become nonsymmetric after passing through a q plate. Also a V point is generated at the center of the beam where the zeros of S_1 , S_2 , and S_3 cross each other. Similarly, simulation results for Stokes vortices for diagonal basis are given in the right column of Fig. 4. For intraconversion of the Stokes index of the S_{23} or S_{31} Stokes vortices, a combination of two QWPs and a q plate can be used. Here referring to Figs. 4(a11)–4(a15) and 4(b11)–4(b15), the combination of

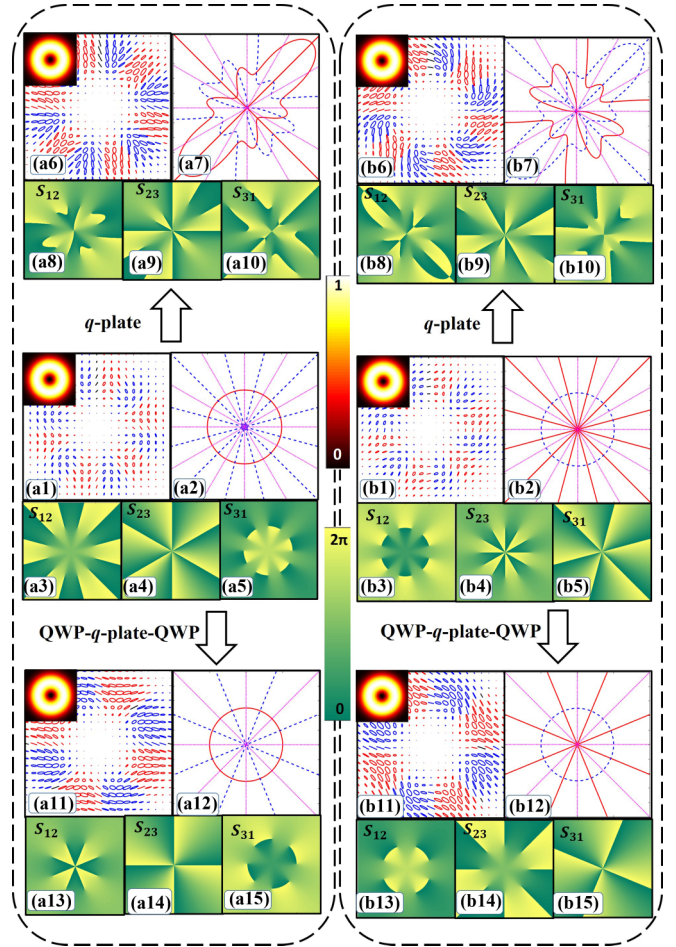


FIG. 4. Use of a q plate alone does not suffice for the inter- or intraconversion of S_{23} and S_{31} Stokes vortices: this is shown by passing the field in Figs. 4(a1) and 4(b1) (middle row) through a q plate with $q = 1/2$ and the output is shown in the top row. Like in Fig. 1, each beam obtained by linear basis superposition has six different attributes. Intraconversion of Stokes vortices is possible by passing the input beam shown in the middle row through a q plate sandwiched between two QWPs. The emerging beam is presented in the bottom row. For incident beam (a1) $u = 2$ and $v = -4$ and (b1) $k = -4$ and $l = 2$, where u , v , k , and l are OAM values carried respective components, in the superposition. All beams are generated for $A = B$ and $\theta_0 = 0$ in Eq. (18).

QWP- q -plate-QWP is useful for intraconversion of $S_{23} \leftrightarrow S_{23}$ and $S_{31} \leftrightarrow S_{31}$ Stokes vortices in linear and diagonal bases, respectively. This is similar to a q plate for intraconversion of $S_{12} \leftrightarrow S_{12}$ Stokes vortices. Depending on the angle of QWPs with a q plate sandwiched in between, the Stokes index of

TABLE I. Different combination of angles of QWPs with a q -plate sandwich in between, for intraconversion of S_{23} Stokes vortices.

S. No.	QWP ₁	QWP ₂	Stokes index
1	$+45^\circ$	$+45^\circ$	$\sigma_{23} + 4q$
2	$+45^\circ$	-45°	$-\sigma_{23} - 4q$
3	-45°	$+45^\circ$	$-\sigma_{23} + 4q$
4	-45°	-45°	$\sigma_{23} - 4q$

TABLE II. Different combination of angles of QWPs with a q -plate sandwich in between, for intraconversion of S_{31} Stokes vortices.

S. No.	QWP ₁	QWP ₂	Stokes index
1	0°	0°	$\sigma_{31} - 4q$
2	0°	90°	$-\sigma_{31} + 4q$
3	90°	0°	$-\sigma_{31} - 4q$
4	90°	90°	$\sigma_{31} + 4q$

S_{23} Stokes vortices can have four different values during intraconversion of S_{23} , as given in Table I. Similarly different combination of angles of QWPs with a q plate sandwiched in between for the intraconversion of S_{31} are given in Table II.

IV. EXPERIMENTAL SETUP AND RESULTS

Experimental setup for verifying the concepts is shown in Fig. 5. It has two sections—one that prepares the beams for carrying out the investigations mentioned in this paper and the other that consists of a block that allows either a q plate or a QWP- q -plate-QWP or a QWP to be inserted into the beam. In the beam generator, a spatially filtered collimated 45° polarized light is launched into the Mach Zehnder type interferometer. This beam is split into two orthogonal polarization components and the two beams follow different arms of the interferometer. A spiral phase plate is inserted in one or both of the arms (with different topological charge) to provide OAM to the respective beam(s) for the generation of bright or dark C point. These two beams are combined by a beam splitter and passed through a QWP to realize superposition in circular basis as given in Eq. (13). The emerging beam contains the S_{12} Stokes vortex at the center. Parameters A

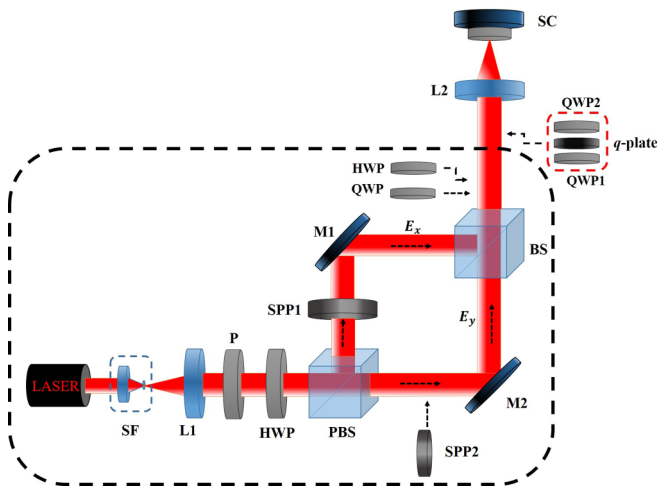


FIG. 5. Experimental setup. The Mach-Zehnder type setup inside the black color rectangle is the Stokes vortex field generator. Intra- and interconversion of Stokes vortices are carried out by either inserting a QWP or by inserting the QWP- q -plate-QWP assembly (red color rectangle) into the beam. Rotation of Stokes vortices is by inserting the q plate into the beam and rotating it. SF, spatial filter assembly; L1, L2, lenses; P, polarizer; PBS, polarizing beam splitter; M1, M2, mirrors; SPP1, SPP2, spiral phase plates; BS, beam splitter; QWP, quarter wave plate; HWP, half wave plate; SC, Stokes camera.

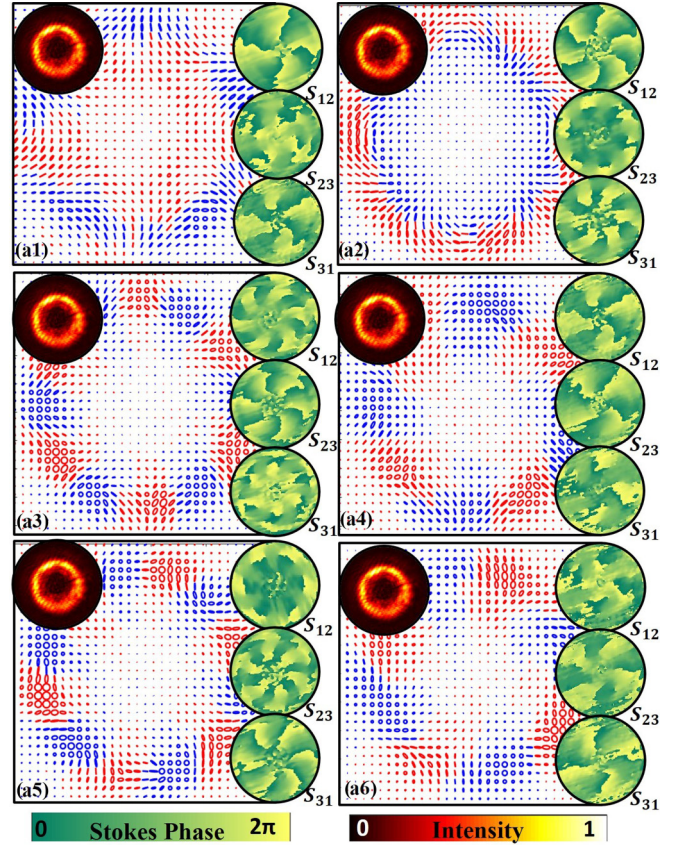


FIG. 6. Experimentally obtained polarization distributions and Stokes phases. Polarization distribution of (a1) incident beam and (a2) transmitted beam, from a q plate of $q = 1/2$, embedded with a c point of $I_c = -2$ and $I_c = +3$, respectively. Panels (a3) and (a5) are the polarization distribution when the beam in (a2) is passed through QWP at 90° and 45°, respectively. Panels (a4) and (a6) depict polarization when (a3) and (a5) is passed through a QWP- q -plate-QWP combination. Inset of each figure shows the intensity and Stokes phases. Here (a1) ↔ (a2), (a3) ↔ (a4), and (a5) ↔ (a6) are intraconversions and (a2) ↔ (a3) and (a2) ↔ (a5) are interconversions.

and B in Eq. (13) can be tuned by rotating a HWP in the beam before the polarizing beam splitter (PBS), which can control the radius of the Stokes ring. For the generation of Stokes vortices due to superposition of beams in the x - y basis, QWP can be removed. Likewise to change the SOPs of the interfering beams to a diagonal basis the QWP can be replaced by a HWP (22.5°) plate.

The generated beam from the assembly shown inside a black dashed rectangle (say generator) is passed through the whole assembly shown in a red dashed rectangle [say converter or element(s) selected from the assembly] for inter- and intraconversion of Stokes vortices. Stokes parameters of the beam are recorded in the far field using a Stokes camera (Salsa Full Stokes camera 1040 × 1040 by Bossa Nova). The measured Stokes parameters are used to obtain polarization distribution and Stokes phases of the beam. Experimental results are given in Fig. 6. Polarization distribution of an emerging beam from the generator embedded with an S_{12} Stokes vortex at the center is depicted in Fig. 6(a1). Polarization distribution of a transmitted beam from a q plate of

$q = 1/2$ is shown in Fig. 6(a2). Stokes phases and intensity are shown as insets in each figure. It can be seen from Fig. 6(a1) and Fig. 6(a2) that Stokes index of S_{12} Stokes vortex changes upon passing through the q plate. Also, there is an increase in the number of S_{23} and S_{31} Stokes vortices. Similarly, polarization distributions of the emerging beam from the generator embedded with S_{23} and S_{31} Stokes vortices at the center are depicted in Figs. 6(a3) and 6(a5), respectively. SOP distributions shown in Figs. 6(a3) and 6(a5) are passed through the combination of QWP- q -plate-QWP assembly and the corresponding SOP distributions are given in Fig. 6(a4) and Fig. 6(a6), respectively.

V. CONCLUSION

In conclusion, we have shown that the q plate can be used for the inter- and intraconversion of Stokes vortices. It is

shown that the number of Stokes vortices embedded in an optical beam can be changed using a q plate which depends on both q value of q plate as well as Stokes index of incident beam; relation for the same is also given. In addition, Stokes vortices can be converted between and among bright and dark intensities by appropriately choosing the q value. Spatial location of Stokes vortices can also be modulated using a q plate. Simulation and experimental results are given to validate the concept. Conservation of sign rules during inter- and intraconversion of Stokes vortices is also validated.

ACKNOWLEDGMENTS

This work has been funded by the Council of Scientific and Industrial Research, India [Files No. 09/086(1323)/2018-EMR-I and No. 03(1430)/18/EMR-II].

-
- [1] L. Allen, M. W. Beijersbergen, R. J. C. Spreeuw, and J. P. Woerdman, Orbital angular momentum of light and the transformation of Laguerre-Gaussian laser modes, *Phys. Rev. A* **45**, 8185 (1992).
 - [2] L. Allen, M. J. Padgett, and M. Babikar, *The Orbital Angular Momentum of Light*, Progress in Optics (Elsevier, Amsterdam, 1999), Vol. 39.
 - [3] I. Freund, A. I. Mokhun, M. S. Soskin, O. V. Angelsky, and I. I. Mokhun, Stokes singularity relations, *Opt. Lett.* **27**, 545 (2002).
 - [4] D. Goldstein, *Polarized Light* (CRC Press, Boca Raton, FL, 2011).
 - [5] W. H. McMaster, Polarization and the Stokes parameters, *Am. J. Phys.* **22**, 351 (1954).
 - [6] S. K. Pal and P. Senthilkumaran, Index polarity inversion by helicity inversion in Stokes vortices, *Appl. Phys. Lett.* **117**, 201101 (2020).
 - [7] Ruchi, P. Senthilkumaran, and S. K. Pal, Phase singularities to polarization singularities, *Int. J. Opt.* **2020**, 2812803 (2020).
 - [8] A. Kosowsky, Cosmic microwave background polarization, *Ann. Phys. (NY)* **246**, 49 (1996).
 - [9] K. H. Kagalwala, H. E. Kondakci, A. F. Abouraddy, and B. E. Saleh, Optical coherency matrix tomography, *Sci. Rep.* **5**, 1 (2015).
 - [10] A. Z. Goldberg, P. de la Hoz, G. Björk, A. B. Klimov, M. Grassl, G. Leuchs, and L. L. Sánchez-Soto, Quantum concepts in optical polarization, *Adv. Opt. Photon.* **13**, 1 (2021).
 - [11] U. Fano, Remarks on the classical and quantum-mechanical treatment of partial polarization, *J. Opt. Soc. Am.* **39**, 859 (1949).
 - [12] J. M. Jauch and F. Rohrlich, *Theory of Photons and Electrons* (Addison-Wesley, Redwood City, CA, 1955).
 - [13] A. I. Akhiezer and V. B. Berestetskii, *Quantum Electrodynamics* (Wiley, New York, 1965).
 - [14] U. Fano, Description of states in quantum mechanics by density matrix and operator techniques, *Rev. Mod. Phys.* **29**, 74 (1957).
 - [15] W. H. McMaster, Matrix representation of polarization, *Rev. Mod. Phys.* **33**, 8 (1961).
 - [16] D. L. Falkoff and J. E. MacDonald, On the Stokes parameters for polarized radiation, *J. Opt. Soc. Am.* **41**, 861 (1951).
 - [17] P. Senthilkumaran, *Singularities in Physics and Engineering* (IOP Publishing, Philadelphia, PA, 2018), pp. 2053–2563.
 - [18] G. Gbur, *Singular Optics*, Series in Optics and Optoelectronics (CRC Press, Boca Raton, FL, 2016).
 - [19] I. Freund, N. Shvartsman, and V. Freilikher, Optical dislocation networks in highly random media, *Opt. Commun.* **101**, 247 (1993).
 - [20] J. F. Annett *et al.*, *Superconductivity, Superfluids and Condensates* (Oxford University Press, Oxford, 2004), Vol. 5.
 - [21] D. J. Griffiths, *Introduction to Electrodynamics* (Pearson, New York, 2013).
 - [22] M. Bahl and P. Senthilkumaran, Helmholtz Hodge decomposition of scalar optical fields, *J. Opt. Soc. Am. A* **29**, 2421 (2012).
 - [23] M. Berry, Phase vortex spirals, *J. Phys. A: Math. Gen.* **38**, L745 (2005).
 - [24] A. Bekshaev and M. Soskin, Transverse energy flows in vectorial fields of paraxial beams with singularities, *Opt. Commun.* **271**, 332 (2007).
 - [25] Ruchi and P. Senthilkumaran, Optical currents in Poincaré beams, *Phys. Rev. A* **102**, 013509 (2020).
 - [26] S. van Enk and G. Nienhuis, Eigenfunction description of laser beams and orbital angular momentum of light, *Opt. Commun.* **94**, 147 (1992).
 - [27] G. Nienhuis and L. Allen, Paraxial wave optics and harmonic oscillators, *Phys. Rev. A* **48**, 656 (1993).
 - [28] V. Kotlyar, S. Khonina, R. Skidanov, and V. Soifer, Rotation of laser beams with zero of the orbital angular momentum, *Opt. Commun.* **274**, 8 (2007).
 - [29] S. K. Pal and P. Senthilkumaran, Synthesis of Stokes vortices, *Opt. Lett.* **44**, 130 (2019).
 - [30] S. Vyas and P. Senthilkumaran, Vortices from wavefront tilts, *Opt. Lasers Eng.* **48**, 834 (2010).
 - [31] S. Vyas and P. Senthilkumaran, Two dimensional vortex lattices from pure wavefront tilts, *Opt. Commun.* **283**, 2767 (2010).
 - [32] A. Khoroshun, O. Chernykh, H. Tatarchenko, S. Sato, Y. Kozawa, A. Popiolek-Masajada, M. Szatkowski, and W. Lamperska, Chain of optical vortices synthesized by a Gaussian beam and the double-phase-ramp converter, *OSA Continuum* **2**, 320 (2019).
 - [33] Y.-N. Hsu and H. H. Arsenault, Optical pattern recognition using circular harmonic expansion, *Appl. Opt.* **21**, 4016 (1982).

- [34] Y.-N. Hsu, H. H. Arsenault, and G. April, Rotation-invariant digital pattern recognition using circular harmonic expansion, *Appl. Opt.* **21**, 4012 (1982).
- [35] I. Freund, Poincaré vortices, *Opt. Lett.* **26**, 1996 (2001).
- [36] I. Freund, Polarization singularity indices in Gaussian laser beams, *Opt. Commun.* **201**, 251 (2002).
- [37] M. Dennis, Polarization singularities in paraxial vector fields: Morphology and statistics, *Opt. Commun.* **213**, 201 (2002).
- [38] A. M. Beckley, T. G. Brown, and M. A. Alonso, Full Poincaré beams, *Opt. Express* **18**, 10777 (2010).
- [39] E. J. Galvez, S. Khadka, W. H. Schubert, and S. Nomoto, Poincaré-beam patterns produced by nonseparable superpositions of Laguerre–Gauss and polarization modes of light, *Appl. Opt.* **51**, 2925 (2012).
- [40] G. Arora, Ruchi, and P. Senthilkumaran, Full Poincaré beam with all the Stokes vortices, *Opt. Lett.* **44**, 5638 (2019).
- [41] Y. I. Salamin, Acceleration in vacuum of bare nuclei by tightly focused radially polarized laser light, *Opt. Lett.* **32**, 3462 (2007).
- [42] Y. Kozawa and S. Sato, Optical trapping of micrometer-sized dielectric particles by cylindrical vector beams, *Opt. Express* **18**, 10828 (2010).
- [43] S. Quabis, R. Dorn, M. Eberler, O. Glöckl, and G. Leuchs, Focusing light to a tighter spot, *Opt. Commun.* **179**, 1 (2000).
- [44] R. Dorn, S. Quabis, and G. Leuchs, Sharper Focus for a Radially Polarized Light Beam, *Phys. Rev. Lett.* **91**, 233901 (2003).
- [45] Q. Zhan and J. R. Leger, Focus shaping using cylindrical vector beams, *Opt. Express* **10**, 324 (2002).
- [46] G. Situ, G. Pedrini, and W. Osten, Spiral phase filtering and orientation-selective edge detection/enhancement, *J. Opt. Soc. Am. A* **26**, 1788 (2009).
- [47] C. T. Samlan, R. R. Suna, D. N. Naik, and N. K. Viswanathan, Spin-orbit beams for optical chirality measurement, *Appl. Phys. Lett.* **112**, 031101 (2018).
- [48] P. Lochab, P. Senthilkumaran, and K. Khare, Designer vector beams maintaining a robust intensity profile on propagation through turbulence, *Phys. Rev. A* **98**, 023831 (2018).
- [49] S. K. Pal and P. Senthilkumaran, Lattice of C points at intensity nulls, *Opt. Lett.* **43**, 1259 (2018).
- [50] L. Marrucci, C. Manzo, and D. Paparo, Optical Spin-to-Orbital Angular Momentum Conversion in Inhomogeneous Anisotropic Media, *Phys. Rev. Lett.* **96**, 163905 (2006).
- [51] G. Machavariani, Y. Lumer, I. Moshe, A. Meir, and S. Jackel, Spatially-variable retardation plate for efficient generation of radially- and azimuthally-polarized beams, *Opt. Commun.* **281**, 732 (2008).
- [52] G. Machavariani, Y. Lumer, I. Moshe, A. Meir, and S. Jackel, Efficient extracavity generation of radially and azimuthally polarized beams, *Opt. Lett.* **32**, 1468 (2007).
- [53] A. Rubano, F. Cardano, B. Piccirillo, and L. Marrucci, Q-plate technology: A progress review (invited), *J. Opt. Soc. Am. B* **36**, D70 (2019).
- [54] Z. Bomzon, G. Biener, V. Kleiner, and E. Hasman, Radially and azimuthally polarized beams generated by space-variant dielectric subwavelength gratings, *Opt. Lett.* **27**, 285 (2002).
- [55] S. Slussarenko, A. Murauski, T. Du, V. Chigrinov, L. Marrucci, and E. Santamato, Tunable liquid crystal q -plates with arbitrary topological charge, *Opt. Express* **19**, 4085 (2011).
- [56] F. Cardano, E. Karimi, S. Slussarenko, L. Marrucci, C. de Lisio, and E. Santamato, Polarization pattern of vector vortex beams generated by q -plates with different topological charges, *Appl. Opt.* **51**, C1 (2012).
- [57] S. Bansal, S. K. Pal, and P. Senthilkumaran, Use of q -plate as a coupler, *Appl. Opt.* **59**, 4933 (2020).
- [58] Z. Liu, Y. Liu, Y. Ke, Y. Liu, W. Shu, H. Luo, and S. Wen, Generation of arbitrary vector vortex beams on hybrid-order Poincaré; sphere, *Photon. Res.* **5**, 15 (2017).
- [59] R. Wang, S. He, S. Chen, J. Zhang, W. Shu, H. Luo, and S. Wen, Electrically driven generation of arbitrary vector vortex beams on the hybrid-order Poincaré; sphere, *Opt. Lett.* **43**, 3570 (2018).
- [60] S. Lou, Y. Zhou, Y. Yuan, T. Lin, F. Fan, X. Wang, H. Huang, and S. Wen, Generation of arbitrary vector vortex beams on hybrid-order Poincaré; sphere based on liquid crystal device, *Opt. Express* **27**, 8596 (2019).
- [61] S. Delaney, M. M. Sánchez-López, I. Moreno, and J. A. Davis, Arithmetic with q -plates, *Appl. Opt.* **56**, 596 (2017).